Synthesis of Titanium Dioxide Nanoparticles for Removal of Pb^{2+}, Cd^{2+} and Cr^{3+} from Wastewater

Hadeel Salah Mansoor[1,2*], Taghried Ali Salman[1], and Saadiyah Ahmed Dhahir[3]

[1]*Department of Chemistry, College of Science, Al-Nahrain University, Baghdad 19002, Iraq*

[2]*Department of Applied Sciences, University of Technology, Baghdad 19002, Iraq*

[3]*Department of Chemistry, College of Science for Women, University of Baghdad, Baghdad 19002, Iraq*

Corresponding author:

email:
hadeel.pchs22@ced.nahrainuniv.edu.iq

Received: December 17, 2024
Accepted: July 8, 2025

DOI: 10.22146/ijc.102753

Abstract: *Water pollution is widely regarded as one of the most pressing global challenges, exacerbated by human progress in industrial, agricultural, and technological sectors. Wastewater often contains non-biodegradable heavy metals that accumulate in living organisms. This accumulation poses significant risks to both environmental ecosystems and human health. The structures and surface morphology were characterized by FTIR, UV-vis measurements, XRD, SEM, and AFM. TiO_2 nanoparticles could remove heavy metal ions (Pb^{2+}, Cd^{2+}, and Cr^{3+}) from two samples (laboratory samples and real samples from Babylon battery factory in Al-Waziriya, Baghdad/Iraq) and measured by AAS. The results indicated that the removal percentages of heavy metal ions by TiO_2 nanoparticles from real sample ions were 91.32, 64.28 and 58.33% for Pb^{2+}, Cd^{2+}, and Cr^{3+}, respectively. The optimum conditions for removal were 0.1 g of TiO_2 nanoparticles, 10 ppm concentration of the pollutant ions, 75 min stirring time, a 100-rpm stirring rate, and a pH level of 7. The kinetic data were related to the pseudo-second-order (R^2 = 0.9455), and the isotherm models were related to the Langmuir equation (R^2 = 0.9769).*

Keywords: *nanoparticles; titanium dioxide; Pb^{2+} pollutant; Cd^{2+} pollutant; Cr^{3+} pollutant*

■ INTRODUCTION

Pollution, defined as any human activity degrading the quality of the natural environment, is one of humanity's most pressing challenges. Environmental degradation, driven by industrialization and urbanization, has reached alarming levels, with heavy metal contamination in water sources emerging as a critical concern [1-2]. Heavy metals such as Cd^{2+}, Cr^{3+}, Pb^{2+}, Hg^{2+}, and As^{3+} are among the most persistent and hazardous pollutants, posing severe risks to human health and ecosystems even at trace concentrations [3]. Prolonged exposure to these metals can lead to detrimental health effects, including neurological disorders, organ damage, and cancer, underscoring the urgent need for effective remediation strategies [4]. Traditional methods for heavy metal removal, such as chemical oxidation, pump-and-treat systems, and thermal treatment, have been widely used but often suffer from limitations such as high costs, inefficiency at low contaminant concentrations, and the generation of secondary pollutants [5].

Recently, nanoremediation has emerged as a promising alternative, leveraging the unique properties of engineered nanomaterials to address these challenges. Nanoremediation offers a more economical, efficient, and environmentally friendly approach to decontaminating polluted sites, particularly for water treatment [6]. Among the various nanomaterials, nanoparticles (NPs) have gained significant attention due to their high surface area, tunable surface chemistry, and exceptional adsorption capacities, making them ideal for the removal of heavy metals through adsorption-based processes [7]. In particular, titanium dioxide (TiO_2) NPs have been extensively studied for

their remarkable properties, including high chemical stability, corrosion resistance, cost-effectiveness, and photocatalytic activity. These attributes make TiO_2 a preferred material for wastewater treatment applications [8]. Recent studies have demonstrated the effectiveness of TiO_2 NPs in adsorbing and degrading a wide range of pollutants, including heavy metals and organic contaminants, from aqueous solutions [9]. However, despite these advancements, gaps remain in optimizing the synthesis methods to enhance the adsorption capacity and selectivity of TiO_2 NPs for specific heavy metals [10-11]. Additionally, these nanomaterials' scalability and long-term stability in real-world applications require further investigation. In this study, we address these gaps by synthesizing TiO_2 NPs via hydrothermal, a technique known for producing highly crystalline and stable nanomaterials. The novelty of this work lies in tailoring TiO_2 NPs to efficiently adsorb heavy metal ions (Pb^{2+}, Cd^{2+}, and Cr^{3+}) from wastewater, addressing gaps in previous research and advancing sustainable nanoremediation technologies.

■ EXPERIMENTAL SECTION

Materials

Titanium tetrachloride ($TiCl_4$) was acquired from Sigma (Sigma–Aldrich, Germany). Lead nitrate ($Pb(NO_3)_2$), cadmium chloride tetrahydrate ($Cd(NO_3)_3{\cdot}4H_2O$), and chromium chloride hexahydrate ($CrCl_3{\cdot}6H_2O$) were acquired from BDH company.

Instrumentation

Fourier transform-infrared (FTIR) was recorded as KBr discs using FTIR-8400S Shimadzu in the range of 4000–400 cm^{-1}. Ultraviolet-visible (UV-vis) single beam spectrophotometer (UV-1100 England) was used for the electronic transitions analysis. Atomic force microscopy (AFM) spectra was measured using atomic force microscopy (SPM-AA 3000). X-ray diffraction (XRD) XRD-7000 was measured in the University of Technology. Scanning electron microscope (SEM) spectra was carried out with a SEM type TE SCAN VEGA, with an accelerating voltage of 30 kV and a magnification of 10000.

Procedure

Preparation of TiO_2 NPs

TiO_2 NPs were prepared by the hydrothermal method (reflux) from $TiCl_4$ as a precursor [12], and a solution consisting of ethanol/deionized water in a volume ratio of 7:3, respectively. The reaction should be carried out in a fume hood or in a round-bottom flask (immersed in an ice bath) for safety purposes. As much as 4 mL of $TiCl_4$ were added to the solution. Then, ethanol/distilled water is added to the round-bottom flask drop by drop over a magnetic stirrer with continuous stirring for 20 min; the solution color converts to white. Then the solution was transferred into a 100 mL stainless-steel autoclave lined with Teflon. The autoclave was sealed and heated in an oven at 200 °C for 6 h. After that, it was kept at room temperature to cool down naturally. The white precipitate of titanium hydroxide formation was washed several times with distilled water, then ethanol, and collected by centrifuge. After that, the precipitate was heated at 100 °C for 1 h to get TiO_2 NPs. The reactions were occurring by following Eq. (1-3) [13];

$$TiCl_4 + 3CH_3CH_2OH + H_2O \xrightarrow[\text{stirring}]{\text{ice bath}} Ti(OCH_2CH_3)_3(OH) \quad (1)$$

$$Ti(OCH_2CH_3)_3(OH) \rightarrow Ti(OH)_4 + 3CH_2CH_2 \quad (2)$$

$$Ti(OH)_4 \rightarrow TiO_2 + 2H_2O \quad (3)$$

Thus, the overall reaction is shown in Eq. (4);

$$TiCl_4 + 3CH_3CH_2OH + H_2O \xrightarrow[\text{2. Heated at 100 } ^oC]{\text{1. Ice bath stirring}} TiO_2 + 4HCl + 3CH_2CH_2 + 2H_2O \quad (4)$$

Preparation of standard metals ions

The Pb^{2+}, Cd^{2+}, and Cr^{3+} metal ions were prepared in stock solution (1000 mg/L) from their salts by dissolving 0.0160 g of $Pb(NO_3)_2$, 0.0274 g of $Cd(NO_3)_3{\cdot}4H_2O$ and 0.0512 g of $CrCl_3{\cdot}6H_2O$.

Preparation of real samples

Application about the removal of heavy metal from real sample ions (wastewater sample collection) from the Babylon battery factory in the Al-Waziriya area in Baghdad, Iraq. To evaluate the analytical suitability of the proposed method and its application for the removal

of some proposed heavy elements from wastewater using prepared TiO_2 NPs, repeated calculation of the concentration of each metal ion and each prepared TiO_2 NPs under the optimum and studied conditions by AAS for each sample.

Applications of removal of Pb^{2+}, Cd^{2+} and Cr^{3+} ions

A batch method was employed to extract Pb^{2+}, Cd^{2+}, and Cr^{3+} ions from laboratory samples. TiO_2 NPs (0.1 g) and 25 mL of each metal ion solution (separately) were mixed and shaken in a rotary shaker at 25 °C with a stirring speed of 150 rpm. The initial concentrations of each Pb^{2+}, Cd^{2+}, and Cr^{3+} ion ranged from 20 to 140 mg/mL. The shaker speed ranged from 50 to 185 rpm. The weight of TiO_2 NPs (0.01–0.10 g), and other parameters were examined to optimize the experimental conditions for removing each ion. Following the establishment of equilibrium was determined. The residual concentration of the metal using AAS and the removal efficiency (%R) of Pb^{2+}, Cd^{2+}, and Cr^{3+} were determined. The best optimization conditions were repeated to determine %R for real samples.

■ RESULTS AND DISCUSSION

FTIR Spectrum for TiO_2 NPs

The FTIR has been widely utilized to detect the different functional groups. Fig. 1(a) displays the spectrum of TiO_2 NPs recorded in the range of 4000–400 cm^{-1}. The bands at 3406 and 1637 cm^{-1} relate to the stretching and deformation vibrations of surface adsorbed water and hydroxyl groups on the surface of TiO_2 NPs. The absence peak at 2900 cm^{-1} in the spectrum of TiO_2 NPs regarding the C–H stretching band means all organic compounds were removed from the samples after washing and heating. These results agree with the reference [14]. The band between 765–447 cm^{-1} is related to Ti–O stretching [15].

UV-vis Spectrum for TiO_2 NPs

The UV-vis or transmittance curve for the TiO_2 NPs heated at 100 °C for 1 h, as shown in Fig. 1(b). Transmittance spectra were measured in the wavelength range of 250–750 nm. The TiO_2 NPs spectrum exhibits high transmittance, up to 385 nm in the UV-vis region. This result corresponds with that for reference [16]. The band gap was calculated using Eq. (5) [17], and found to be 3.22 eV, at λ_{max} equal to 386 nm;

$$\text{Energy gap} = \frac{1240}{\lambda_{max}} \quad (5)$$

where 1240 is a factor to change nm to eV, and λ_{max} is the maximum of transmission (nm) [18].

XRD for TiO_2 NPs

Cu Kα radiation (λ = 1.5405 Å) has been employed in the diffraction of X-rays to characterize TiO_2 NPs, as shown in Fig. 2. The XRD spectrum was obtained by scanning 2θ within the 20–80° range. The diffraction peaks of TiO_2 NPs heated at a temperature of 100 °C for

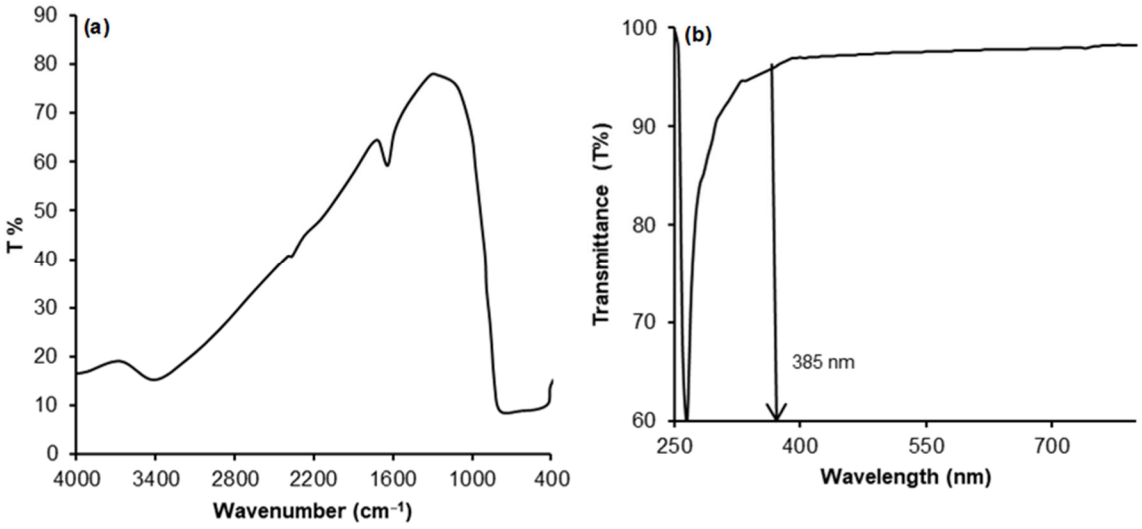

Fig 1. (a) FTIR spectrum and (b) optical transmittance for TiO_2 NPs

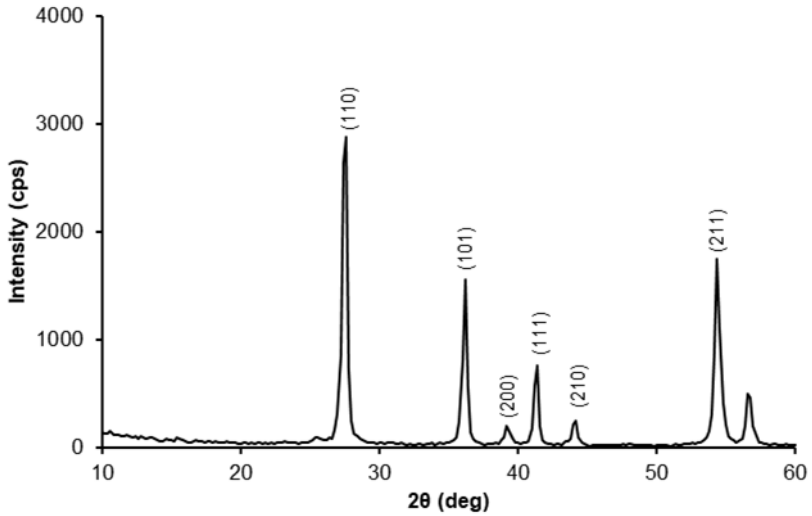

Fig 2. XRD of TiO_2 NPs

1 h, are (110), (101), (200), (111), (210), and (211) at 2θ = 27.52, 36.19, 39.26, 41.33, 44.12, and 54.40° which are indexed in the JCPDS card no. 21-1276 and appear in the rutile form [19-20].

AFM and SEM for TiO_2 NPs

Fig. 3(a) and 3(b) show a typical three-dimensional AFM image and the granularity accumulation distribution chart of TiO_2 NPs. The average grain size was found to be 71.35 nm. The morphological investigation of TiO_2 NPs was done using SEM analysis. Fig. 3(c) displays the SEM pictures of TiO_2 NPs that were heated for 1 h at 100 °C using the hydrothermal technique of preparation. Based on the morphology of TiO_2 NPs, there are nanosphere shapes (~86 nm) [21].

Effect of Adsorbent Dosage

While conducting measurements using an AAS, a calibration curve and straight-line equation was obtained for the ions Pb^{2+}, Cd^{2+}, and Cr^{3+} with a concentration range of 2, 4, 6, 8, 10, 12, and 14 mg/mL at λ_{max} 217, 228, and 357 of Pb^{2+}, Cd^{2+}, and Cr^{3+}, respectively. In adsorption dosage, the capacity of an adsorbent for a specific starting concentration is determined by the adsorbent dosage. Fig. 4 illustrates the effects of a TiO_2 NPs adsorbent dosage on the removal of Pb^{2+}, Cd^{2+}, and Cr^{3+} ions at 4 mg/L. It was noted that when the dosage was increased from 0.01 to 0.1 g, because the optimum weight used was 0.1 g in all of these experimental studies, the removal percent of each

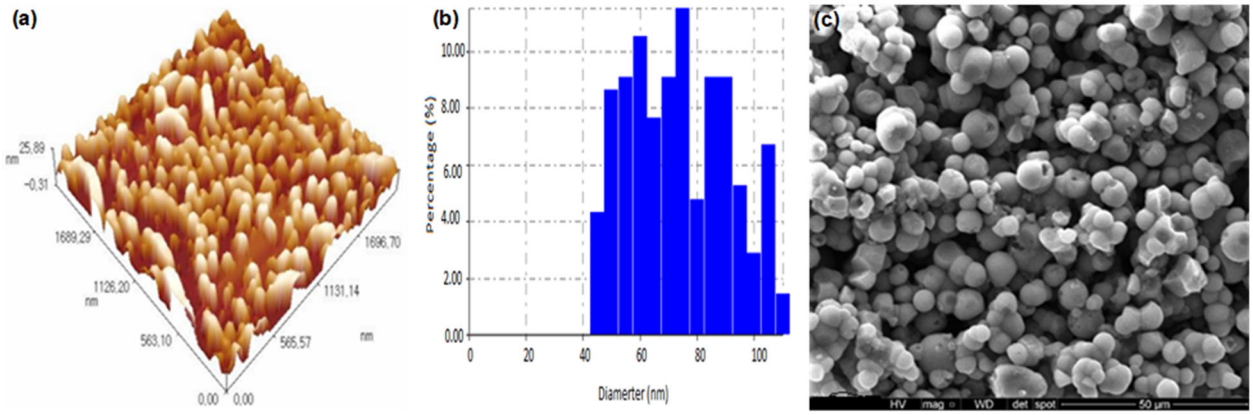

Fig 3. (a) 3D AFM, (b) size distribution charts, and (c) SEM image of TiO_2 NPs

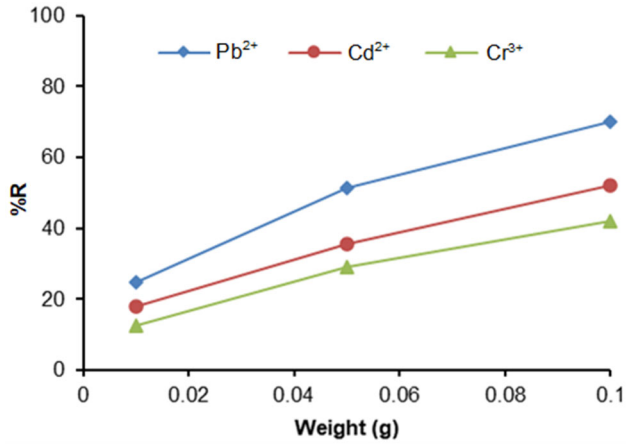

Fig 4. Effect of TiO_2 NPs dose on Pb^{2+}, Cd^{2+}, and Cr^{3+} adsorption

metal increased quickly, resulting in efficient and consistent outcomes across the board.

The %R of heavy metal ions was computed by dividing the removed heavy metal concentration by the initial concentration value as shown in Eq. (6);

$$\%R = \left[\frac{C_0 - C_t}{C_0}\right] \times 100\% \quad (6)$$

where C_0 is the initial heavy metal concentration (mg/mL) and C_t is the heavy metal concentration at time t (mg/mL).

$$q_t = \left[\frac{C_0 - C_t}{w}\right] \times V \quad (7)$$

Eq. (7) shows the calculation of adsorption capability, where V is solution volume (L), w is adsorbent weight (g), and q_t (mg/g) is heavy metal adsorption capability following solution-adsorbent contact time [22].

The effect of contact time of Pb^{2+}, Cd^{2+}, and Cr^{3+} ions

Throughout a long period of time, removal efficiency increases at varying rates. For the removal of Pb^{2+}, Cd^{2+}, and Cr^{3+}, the first stage took 30, 45, 60, 75, and 90 min, respectively. The maximum removal percent required 75 min (Fig. 5). After that, the uptake of all the metal ions slowed down and ultimately stopped growing. This can be explained by increasing the time; the adsorption became the best possible at 75 min. Increasing the time does not affect the concentration as a result of the completion of the adsorption process.

The effect of initial pollutant concentration

The study investigated the removal efficiency of Pb^{2+}, Cd^{2+}, and Cr^{3+} ions at varying initial concentrations (2–14 mg/mL) and found that 10 mg/mL was the optimal concentration for maximum removal. The adsorbent surface becomes fully saturated at this concentration, allowing the highest percentage of metal ions to bind effectively. However, when the concentration exceeds 10 mg/mL, the surface becomes supersaturated, leading to competition for binding sites and causing some ions to detach, which reduces removal efficiency (Fig. 6). This behavior is attributed to the limited capacity of the adsorbent, where exceeding its saturation point results in decreased performance due to the instability of the supersaturated surface [23].

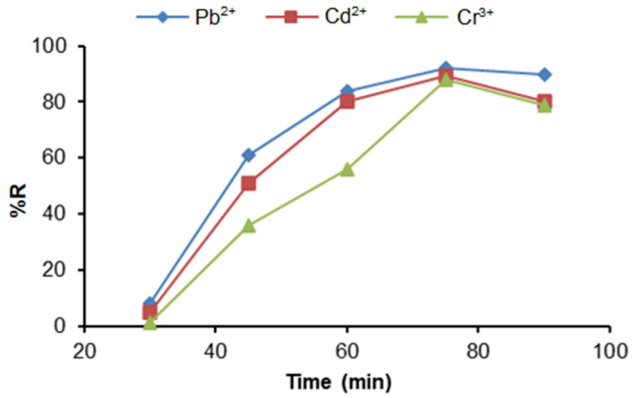

Fig 5. Effect of shaking time on the removal of Pb^{2+}, Cd^{2+}, and Cr^{3+} using TiO_2 NPs

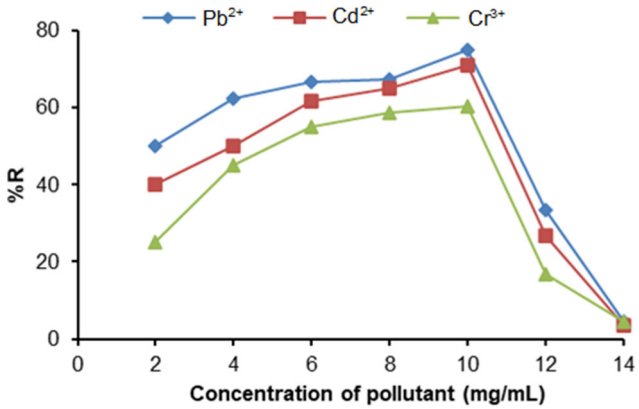

Fig 6. Effect of initial Pb^{2+}, Cd^{2+}, and Cr^{3+} concentrations on their adsorption using TiO_2 NPs

The effect of the shaking at different speeds

The study examined the effect of shaking speed (50, 100, 150, and 185 rpm) on the adsorption of Pb^{2+}, Cd^{2+}, and Cr^{3+} ions over 75 min and found that 100 rpm was the optimal speed for achieving the highest removal efficiency. At this speed, the increased kinetic energy and collision frequency enhance the adhesion of metal ions to the adsorbent surface, maximizing their binding. However, when the shaking speed exceeds 100 rpm, the excessive kinetic energy causes some of the adsorbed ions to detach from the surface, reducing the overall removal efficiency (Fig. 7). This occurs because the higher energy disrupts the stability of the adsorbed particles, leading to their release back into the solution. Thus, 100 rpm represents the balance between effective adsorption and the destabilizing effects of excessive shaking.

The effect of the solution pH

The study explored the effect of pH on the adsorption of Pb^{2+}, Cd^{2+}, and Cr^{3+} ions using TiO_2 NPs, as pH plays a crucial role in determining the surface properties of the adsorbent and the chemical state of the metal ions in solution. Experiments were conducted across a broad pH range of 3 to 13 to analyze its impact on removal efficiency, as illustrated in Fig. 8. The results showed that the removal efficiency for Pb^{2+}, Cd^{2+}, and Cr^{3+} increased with rising pH values, reaching its maximum at pH = 7. This optimal performance at neutral pH is attributed to the adsorbent surface being in a neutral state, providing ideal conditions for binding metal ions. However, beyond pH 7, the removal efficiency declined. This decrease is likely due to the adsorbent surface becoming more negatively charged at higher pH values, reducing its ability to attract positively charged metal ions. Additionally, metal ions at alkaline pH levels tend to form hydroxides, reducing their availability for adsorption. Thus, pH 7 represents the optimal condition for maximizing the adsorption of Pb^{2+}, Cd^{2+}, and Cr^{3+} by TiO_2 NPs [24].

Application of the Removal of Heavy Metal from Wastewater Samples

Wastewater samples were collected from the washing process effluent of the Babylon battery factory in Al-Waziriya, Baghdad. After filtration to remove suspended impurities, the initial Pb^{2+}, Cd^{2+}, and Cr^{3+} concentrations were quantified using atomic absorption spectroscopy. TiO_2 NPs were introduced into the wastewater under optimized conditions (0.1 g dosage, 10 ppm concentration, 75 min stirring at 100 rpm, and pH 7) to assess their adsorption efficiency. Fig. 9 presents the post-treatment results, highlighting the removal efficacy of TiO_2 NPs for each heavy metal (91.32% Pb^{2+}, 64.28% Cd^{2+}, and 58.33% Cr^{3+}). These findings confirm the practical viability of TiO_2 NPs for industrial wastewater remediation, particularly in battery manufacturing effluents laden with toxic metals. After treatment with TiO_2 NPs, the adsorption process results are presented in Fig. 9, which likely shows the effectiveness of TiO_2 NPs in removing Pb^{2+}, Cd^{2+}, and Cr^{3+} from the wastewater.

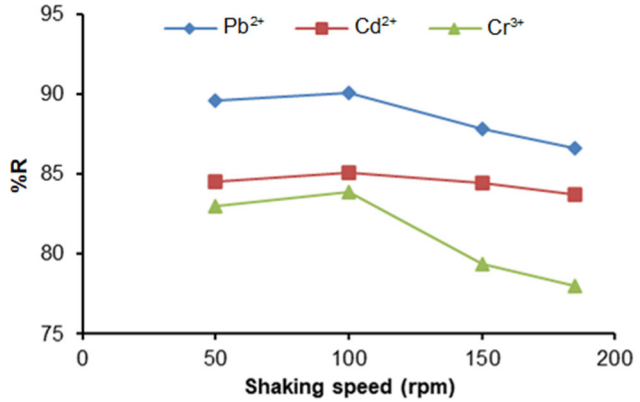

Fig 7. Effect of shaking at different speeds on the removal of Pb^{2+}, Cd^{2+}, and Cr^{3+} using TiO_2 NPs

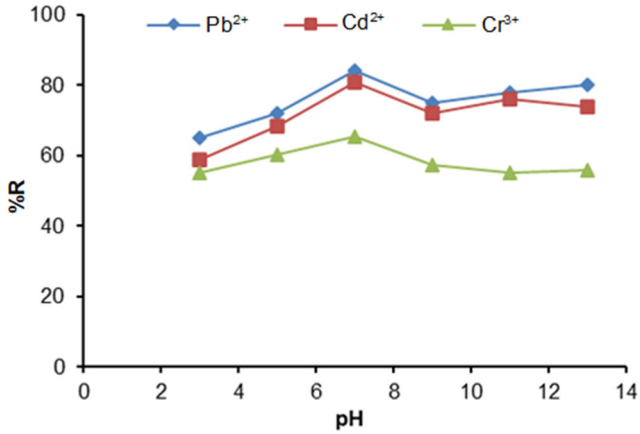

Fig 8. Effect of the solution pH on the removal of Pb^{2+}, Cd^{2+}, and Cr^{3+} using TiO_2 NPs

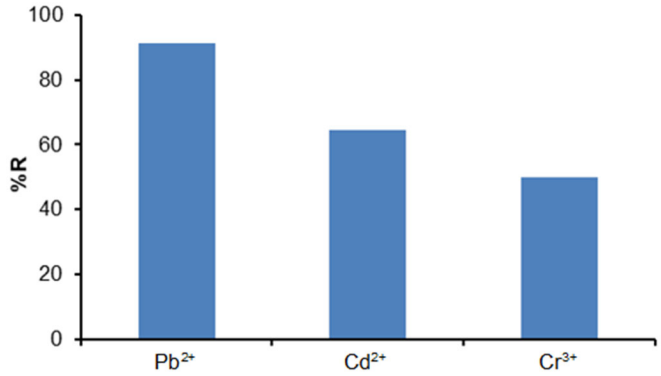

Fig 9. Removal of Pb^{2+}, Cd^{2+}, and Cr^{3+} from wastewater sample

This step demonstrates the practical application of TiO_2 NPs for heavy metal removal in industrial wastewater treatment.

Kinetic and Isotherm Adsorption Models

Kinetic adsorption of Pb^{2+} ions

The study conducted kinetic analyses to understand the adsorption behavior of Pb^{2+} on TiO_2 NPs, as the TiO_2 NPs sample exhibited strong adsorption capabilities for Pb^{2+} removal [25]. The amount of Pb^{2+} adsorbed by the TiO_2 NPs sample was observed to change over time, as shown in Fig. 10(a). Initially, the adsorption process was rapid during the first 75 min, indicating a high rate of Pb^{2+} uptake by the TiO_2 NPs surface. However, as the surface of the TiO_2 NPs became increasingly saturated with adsorbed Pb^{2+} ions, the rate of adsorption slowed down [26]. This is typical in adsorption processes, where the availability of active sites decreases as they become occupied. The system reached adsorption equilibrium after approximately 90 min, meaning no further significant adsorption occurred beyond this point [27].

To further analyze the adsorption kinetics, three kinetic models were applied to the data, i.e., pseudo-first-order, pseudo-second-order, and Weber–Morris intraparticle diffusion model.

Pseudo-first-order model. This model assumes that the rate of adsorption is proportional to the number of unoccupied adsorption sites. It is expressed by the Eq. (8);

$$\log(q_e - q_t) = \log q_e - k_1 \frac{t}{2.303} \quad (8)$$

where q_e is the amount of Pb^{2+} adsorbed at equilibrium, q_t is the amount adsorbed at time t, and k_1 is the rate constant of the pseudo-first-order model. The study likely compared the experimental data with these models to determine which one best describes the adsorption process, providing insights into the mechanism and rate of Pb^{2+} removal by TiO_2 NPs.

Pseudo-second-order model. This model assumes that the rate of adsorption is proportional to the square of the number of unoccupied adsorption sites. It is expressed by Eq. (9) [28];

$$\frac{t}{q_t} = \frac{1}{k_2 q_e^2} + \frac{t}{q_e} \quad (9)$$

where k_2 is the equilibrium rate constant of the pseudo-second-order model (in g/mg·min).

Weber–Morris intraparticle diffusion model. This model describes the diffusion of adsorbate (Pb^{2+}) into the pores of the adsorbent (TiO_2 NPs). It is expressed by Eq. (10) [29];

$$q_t = k_d (t)^{0.5} + C \quad (10)$$

k_d is the intraparticle diffusion rate constant (in mg/g·min$^{1/2}$), and C is a constant related to the boundary layer effect [30].

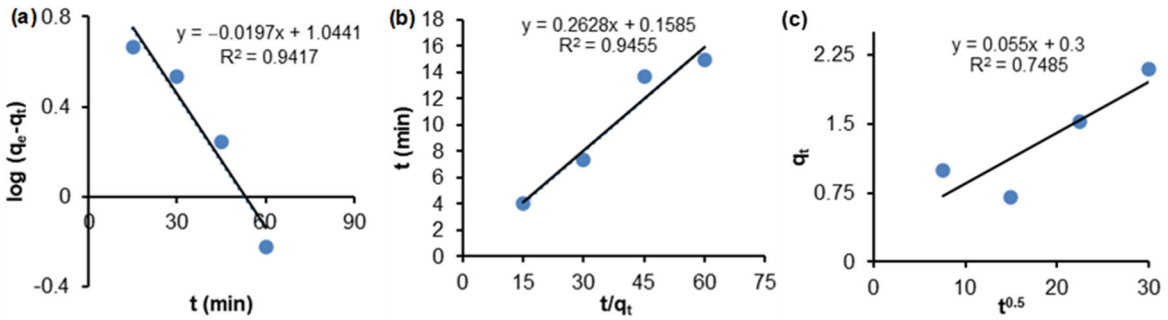

Fig 10. (a) pseudo-first-order, (b) pseudo-second-order, and (c) intra-particle diffusion plot for Pb^{2+} adsorption onto TiO_2 NPs

The pseudo-first-order model yielded an R^2 value of 0.9417 (Fig. 10(a)), indicating a good fit but not the best. The pseudo-second-order model provided a better fit with an R^2 value of 0.9455 (Fig. 10(b)), suggesting that this model more accurately describes the adsorption process. This implies that the rate-limiting step in Pb^{2+} adsorption is likely physisorption, involving weak interactions between Pb^{2+} ions and the TiO_2 surface, which agrees with the references [31-33].

The Weber–Morris intraparticle diffusion model was used to investigate the diffusion mechanism. The value of C from Eq. (10) indicated the presence of a boundary layer effect, meaning that surface adsorption and diffusion both play roles in the rate-controlling step. The increase in C values (Fig. 10(c) and Table 1) suggests that the boundary layer thickness increases during the adsorption process [34], further supporting the contribution of surface adsorption in the rate control step.

Isotherm adsorption

Since the Langmuir and Freundlich equation models describe the adsorption behavior of heavy element ions on the surface of nano oxides, they will be used to comprehend and assess the adsorption process. The maximal capacity for ion adsorption on a certain surface of a nano oxide at equilibrium is found using the Langmuir equation, as well as being aware of the surface's characteristics, such as its roughness and chemical makeup, and the kind of adsorption, such as chemical or physical adsorption. The adsorption takes place on homogeneous sites in a monolayer pattern if the results match the Langmuir equation (Eq. (11)). On the other hand, if the results match the Freundlich equation, the nano oxide's surface is not homogeneous, and the adsorption may be multilayer (Eq. (12)), with variations in adsorption energies at different sites [35]. The free energy of adsorption is calculated based on Eq. (13);

$$\frac{C_e}{q_e} = \frac{1}{K_L q_{max}} + \frac{C_e}{q_{max}} \quad (11)$$

$$\log q_e = \log K_F + \frac{1}{n}\log C_e \quad (12)$$

$$\Delta G^\circ = -RT\ln(K) \quad (13)$$

where K_L is the Langmuir adsorption equilibrium constant (L/mg). C_e, q_e, and q_{max} are the residual heavy metal ion concentrations in solution (mg/L), the amount of heavy metal ion adsorbed (mg/g) on the sorbent at equilibrium, and the maximum amount of the heavy metal per unit weight of sorbent (mg/g). The Freundlich adsorption constant and the adsorption intensity are denoted by K_F and n, respectively. R, T, and K represent the gas constant (8.314 J/mol K), absolute temperature, and K equilibrium constant for Freundlich or Langmuir, respectively [36]. Based on Fig. 11(a) and 11(b), the Langmuir model has a higher R^2 (0.9769) compared to the Freundlich model (R^2 = 0.6925); the system likely follows monolayer adsorption on a homogeneous surface. This suggests that all adsorption sites are equivalent and

Table 1. Comparison of the kinetic model equations on the adsorption of Pb^{2+} from solution

Pseudo-first-order			Pseudo-second-order			Intra-particle diffusion		
k_1 (min^{-1})	q_e calc (mg/g)	R^2	k_2 (g/mg min)	q_e calc (mg/g)	R^2	k_d (mg/g $min^{1/2}$)	C	R^2
0.04536	11.068	0.9417	0.4357	3.8051	0.9455	0.055	0.3	0.7485

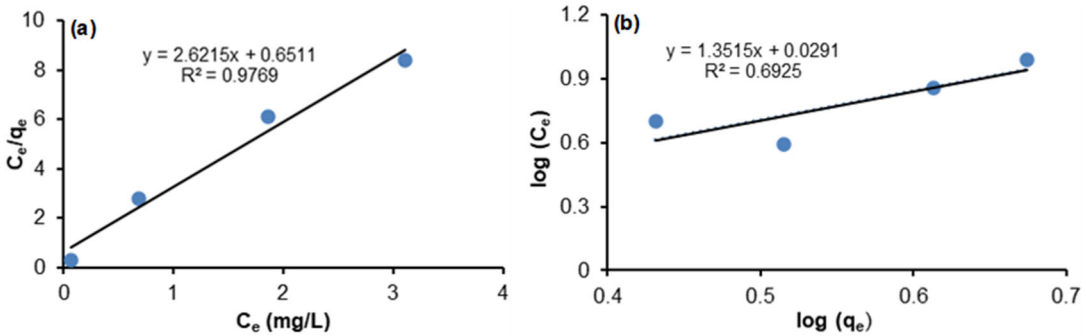

Fig 11. (a) Langmuir and (b) Freundlich isotherm adsorption of TiO_2 NPs

Table 2. Comparison of the Langmuir and Freundlich models on the Pb^{2+} adsorption from the solution

Langmuir				Freundlich			
q_{max} (min^{-1})	K_L (L/mg)	R^2	$\Delta G_L°$ (kJ/mol)	K_F (mg/g)	n	R^2	$\Delta G_F°$ (kJ/mol)
0.3814	4.0262	0.9769	−3.450	1.069	0.7399	0.6925	−0.165

confirms that the adsorption is physically favorable (n < 1) (Table 2). This result agrees with the references results of [31,33,37-38].

■ CONCLUSION

In this work, TiO_2 NPs were successfully prepared and characterized by different methods such as XRD, AFM, SEM, FTIR, and UV-vis spectrophotometer. The average grain size of TiO_2 NPs was 71.35 nm, and the shapes of the nanoparticles were nanoflakes. These TiO_2 NPs were used to remove three types of metal ions (Pb^{2+}, Cd^{2+}, and Cr^{3+}) from wastewater. They were shown to be very successful adsorbents for removing these metal ions from wastewater using AAS. The optimum conditions were determined and found to be 0.1 g of absorbent, 10 mg/mL of pollutants, 75 min of contact time, 100 rpm of shake speed, and pH of 7 at 25 °C. The %R and q_t for Pb^{2+} were higher in all cases. The pseudo-second-order model fit the experimental results on Pb^{2+} adsorption, while the Langmuir isotherm equation is a better fit than the Freundlich isotherm model, and $\Delta G_F°$ was −3.45 kJ/mol, which is more spontaneous than the Langmuir model. The type of interaction is physical interaction.

■ ACKNOWLEDGMENTS

We extend our thanks and gratitude to the co-researchers who contributed to my completing the research at the scientific laboratories at Al-Nahrain University of the Chemistry Department, where the experiments were conducted.

■ CONFLICT OF INTEREST

The authors declare that they have no known competing financial interests or personal relationships that could have appeared to influence the work reported in this manuscript.

■ AUTHOR CONTRIBUTIONS

All authors contributed to the study's conception and design. Hadeel Salah Mansoor, Taghried Ali Salman, and Saadiyah Ahmed Dhahir performed the material preparation, data collection, and analysis. Hadeel Salah Mansoor wrote the first draft of the manuscript, and all authors commented on previous versions. All authors read and approved the final manuscript.

■ REFERENCES

[1] Akhtar, N., Syakir Ishak, M.I., Bhawani, S.A., and Umar, K., 2021, Various natural and anthropogenic factors responsible for water quality degradation: A review, *Water*, 13 (19), 2660.

[2] Briffa, J., Sinagra, E., and Blundell, R., 2020, Heavy metal pollution in the environment and their toxicological effects on humans, *Heliyon*, 6 (9), e04691.

[3] Khanam, R., Kumar, I., Oladapo-Shittu, O., Twose, C., Islam, A.S.M.D.A., Biswal, S.S., Raqib, R., and Baqui, A.H., 2021, Prenatal environmental metal exposure and preterm birth: A scoping review, *Int. J. Environ. Res. Public Health*, 18 (2), 573.

[4] Akash, M.S.H., Yaqoob, A., Rehman, K., Imran, M., Assiri, M.A., Al-Rashed, F., Al-Mulla, F., Ahmad, R., and Sindhu, S., 2023, Metabolomics: A promising tool for deciphering metabolic impairment in heavy metal toxicities, *Front. Mol. Biosci.*, 10, 1218497.

[5] Jadaa, W., and Mohammed, H.K., 2023, Toxic heavy metals elimination from contaminated effluents utilizing various adsorbents: Critical mini-review, *J. Biomed. Res. Environ. Sci.*, 4 (2), 281–296.

[6] Restrepo, C.V., and Villa, C.C., 2021, Synthesis of silver nanoparticles, influence of capping agents, and dependence on size and shape: A review, *Environ. Nanotechnol., Monit. Manage.*, 15, 100428.

[7] Yang, J., Hou, B., Wang, J., Tian, B., Bi, J., Wang, N., Li, X., and Huang, X., 2019, Nanomaterials for the removal of heavy metals from wastewater, *Nanomaterials*, 9 (3), 424.

[8] Kumar, S.G., and Devi, L.G., 2011, Review on modified TiO_2 photocatalysis under UV/visible light: Selected results and related mechanisms on interfacial charge carrier transfer dynamics, *J. Phys. Chem. A*, 115 (46) 13211–13241.

[9] Bhuyan, M.A.H., Gebre, R.K., Finnilä, M.A.J., Illikainen, M., and Luukkonen, T., 2022, Preparation of filter by alkali activation of blast furnace slag and its application for dye removal, *J. Environ. Chem. Eng.*, 10 (1), 107051.

[10] Ghareeb, A., Fouda, A., Kishk, R.M., and El Kazzaz, W.M., 2024, Unlocking the potential of titanium dioxide nanoparticles: An insight into green synthesis, optimizations, characterizations, and multifunctional applications, *Microb. Cell Fact.*, 23 (1), 341.

[11] Engates, K.E., and Shipley, H.J., 2011, Adsorption of Pb, Cd, Cu, Zn, and Ni to titanium dioxide nanoparticles: Effect of particle size, solid concentration, and exhaustion, *Environ. Sci. Pollut. Res.*, 18 (3), 386–395.

[12] Wang, W., and Wang, A., 2019, "Palygorskite Nanomaterials: Structure, Properties, and Functional Applications" in *Nanomaterials from Clay Minerals*, Elsevier, Amsterdam, Netherlands, 21–133.

[13] Rasheed, R.T., Mansoor, H.S., Al-Shaikhly, R.R., Abdullah, T.A., Salman, A.D., and Juzsakova, T., 2020, Synthesis and catalytic activity studies of α-MnO_2 nanorodes, rutile TiO_2 and its composite prepared by hydrothermal method, *AIP Conf. Proc.*, 2213 (1), 020122.

[14] Rajaram, P., Jeice, A.R., and Jayakumar, K., 2024, Influences of calcination temperature on titanium dioxide nanoparticles synthesized using *Averrhoa carambola* leaf extract: *In vitro* antimicrobial activity and UV-light catalyzed degradation of textile wastewater, *Biomass Convers. Biorefin.*, 14 (17), 20665–20678.

[15] Ba-Abbad, M.M., Kadhum, A.A.H., Mohamad, A.B., Takriff, M.S., and Sopian, K., 2020, Synthesis and catalytic activity of TiO_2 nanoparticles for photochemical oxidation of concentrated chlorophenols under direct solar radiation, *Int. J. Electrochem. Sci.*, 15, 8321–8336.

[16] Giampiccolo, A., Tobaldi, D.M., Jones, E., Labrincha, J.A., Kurchania, R., Ansell, M.P., and Ball, R.J., 2021, UV/visible sol gel W–TiO_2 photocatalytic coatings for interior building surfaces, *Build. Environ.*, 205, 108203.

[17] Gareso, P.L., Heryanto, H., Juarlin, E., and Taba, P., 2022, Effect of annealing on the structural and optical properties of ZnO/ITO and AZO/ITO thin films prepared by sol-gel spin coating, *Trends Sci.*, 20 (3), 6521.

[18] Hussein, E.A., and Kareem, S.H., 2020, Magnetic mesoporous silica material (Fe_3O_4@$mSiO_2$) as adsorbent and delivery system for ciprofloxacin drug, *IOP Conf. Ser.: Mater. Sci. Eng.*, 871 (1), 012020.

[19] Podelinska, A., Neilande, E., Pankratova, V., Serga, V., Bandarenka, H., Burko, A., Piskunov, S., Pankratov, V.A., Sarakovskis, A., Popov, A.I., and Bocharov, D.V., 2025, Structural and spectroscopic characterization of TiO_2 nanocrystalline materials synthesized by different methods, *Nanomaterials*, 15 (7), 498.

[20] Rasheed, R.T., Mansoor, H.S., and Qasim, B.H., 2019, Antibacterial activity of TiO_2 and TiO_2 composites nanopowders prepared by hydrothermal method, *Mater. Res. Express*, 6 (8), 0850a5.

[21] Shakeel, N., Piwoński, I., Kisielewska, A., Krzywiecki, M., Batory, D., and Cichomski, M., 2024, Morphology-dependent photocatalytic activity of nanostructured titanium dioxide coatings with silver nanoparticles, *Int. J. Mol. Sci.*, 25 (16), 8824.

[22] Osama, H.R., Mohamed, A.A., and Ashraf, A.M., 2021, An eggshell hydroxyapatite-graphene oxide nanocomposite for the removal of heavy metals from waste water, *J. Environ. Sci.*, 50 (2), 1–33.

[23] Dawwam, G.E., Abdelfattah, N.M., Abdel-Monem, M.O., Jahin, H.S., Omer, A.M., Abou-Taleb, K.A., Mansor, E.S., 2023, An immobilized biosorbent from *Paenibacillus dendritiformis* dead cells and

polyethersulfone for the sustainable bioremediation of lead from wastewater, *Sci. Rep.*, 13 (1), 891.

[24] Maneechakr, P., and Mongkollertlop, S., 2020, Investigation on adsorption behaviors of heavy metal ions (Cd^{2+}, Cr^{3+}, Hg^{2+} and Pb^{2+}) through low-cost/active manganese dioxide-modified magnetic biochar derived from palm kernel cake residue, *J. Environ. Chem. Eng.*, 8 (6), 104467.

[25] Sruamsiri, D.A., and Ogawa, M., 2022, Adsorption of Pb^{2+} on a layered alkali titanate from water, *IOP Conf. Ser.: Earth Environ. Sci.*, 950 (1), 012040.

[26] Smith, D.M., Hamwi, B., and Rogers, R.E., 2022, Carbon nanomaterial-based aerogels for improved removal of copper(II), zinc(II), and lead(II) ions from water, *Environ. Sci.: Adv.*, 1 (2), 208–215.

[27] Raveesh, G., Goyal, R., and Tyagi, S.K., 2025, Sugarcane bagasse derived composite sorbent for sorption based atmospheric water harvesting, *Sep. Purif. Technol.*, 356 (Pt A), 129820.

[28] Dal, M.C., and Onursal, N., 2023, Two new linearized equations derived from the pseudo-second-order kinetic model, *Desalin. Water Treat.*, 308, 183–189.

[29] Lee, J.J., 2021, Characteristics of equilibrium, kinetics and thermodynamics for adsorption of disperse yellow 3 dye by activated carbon, *Clean Technol.*, 27 (2), 182–189.

[30] Basuki, R., Wijaya, S., Kusumastuti, A., and Amalia, R., 2021, The dependency of kinetic parameters as a function of initial solute concentration: New insight from adsorption of dye and heavy metals onto humic-like modified adsorbents, *Bull. Chem. React. Eng. Catal.*, 16 (4), 773–795.

[31] Poursani, A.S., Nilchi, A., Hassani, A., Shariat, S.M., and Nouri, J., 2016, The synthesis of nano TiO_2 and its use for removal of lead ions from aqueous solution, *J. Water Resour. Prot.*, 8 (4), 438–448.

[32] Ali, A.A., Elfiky, E.M., Ahmed, I.S., Khalil, A.A., and Mohamed, T.Y., 2020, Auto-combustion fabrication and characterization of TiO_2 nanoparticles and utilization as an adsorbent for removal of Pb^{2+} from aqueous solution, *Desalin. Water Treat.*, 193, 83–94.

[33] Parastoosadeghi, P., Rezaei, H., and Hedayati, S.A., 2016, Thermodynamic and kinetic studies for the adsorption of Cd(II) using nanoparticles of TiO_2 from aqueous solution, *Chem. Technol.: Indian J.*, 11 (4), 149–158.

[34] Hashem, A., Aniagor, C.O., Taha, G.M., and Fikry, M., 2021, Utilization of low-cost sugarcane waste for the adsorption of aqueous Pb(II): Kinetics and isotherm studies, *Curr. Res. Green Sustainable Chem.*, 4, 100056.

[35] Damiri, F., Andra, S., Kommineni, N., Balu, S.K., Bulusu, R., Boseila, A.A., Akamo, D.O., Ahmad, Z., Khan, F.S., Rahman, M.H., Berrada, M., and Cavalu, S., 2022, Recent advances in adsorptive nanocomposite membranes for heavy metals ion removal from contaminated water: A comprehensive review, *Materials*, 15 (15), 5392.

[36] Zaki, E.R., Ahmed, S.M., Ali, O.I., and Abdalla, M.S., 2022, Adsorption properties of magnetite nanoparticles for the removal of heavy metals from aqueous solution, *Egypt. J. Appl. Sci.*, 37 (5-6), 11–29.

[37] Motlochová, M., Slovák, V., Pližingrová, E., Lidin, S., and Šubrt, J., 2020, Highly-efficient removal of Pb(II), Cu(II) and Cd(II) from water by novel lithium, sodium and potassium titanate reusable microrods, *RSC Adv.*, 10 (7), 3694–3704.

[38] Hang, Y., Yin, H., Wang, A., Shen, L., Feng, Y., and Liu, R., 2014, Preparation of titanate whiskers starting from metatitanic acid and their adsorption performances for Cu(II), Pb(II), and Cr(III) ions, *Water, Air, Soil Pollut.*, 225 (9), 2095.